6 Satellite Links

6.1 Introduction

Satellite links, operating either between the Earth and a satellite or the other way round, are characterised by an oblique direction of propagation. For this reason, compared with terrestrial links operating between two points located at the surface of the Earth, the study of the propagation of radio waves in this case is to some extent simplified. For instance, the influence of the ground can be neglected, thus allowing for the elimination of ground reflection and diffraction phenomena. Further, since waves generally propagate inside atmospheric layers at angles higher than a few degrees, atmospheric paths can be for the most part eliminated.

Therefore, the study of radio wave propagation between the Earth and a satellite comes down, besides free-space attenuation, to the study of phenomena related to the refractive indexes inside the troposphere and the ionosphere, to the absorption due to atmospheric gases, oxygen and water vapour in particular, and to the attenuation caused by hydrometeors like clouds, rain, fog, snow or ice.

6.2 Free-Space Attenuation

Attenuation in free-space, also referred to as transmission loss, is due to the dispersion of energy which takes place as the wave travels away from the transmitter. It is defined by the equation:

$$A_0 = -20\log_{10}\left(\frac{\lambda}{4\pi d}\right) = 32.4 + 20\log_{10}(f) + 20\log_{10}(d) \qquad (6.1)$$

where A_0 is the free-space attenuation (dB), λ is the wavelength in kilometres, d is the distance in kilometres travelled between the transmitter and the receiver and f is the frequency in MHz.

Distances being generally large, the attenuation values for space links are relatively high compared with values obtained in the case of line-of-sight radio relay systems. The difference is about 50 dB, as can be seen in Fig. 6.1.

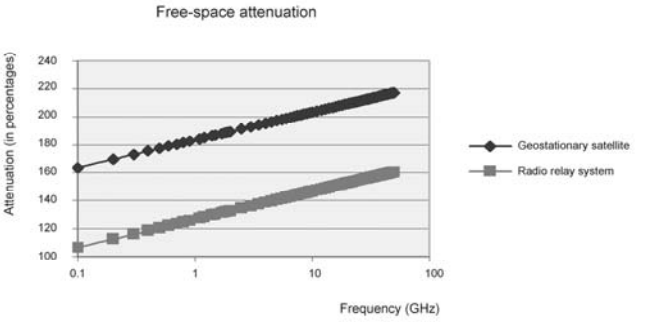

Fig. 6.1. Attenuation in free-space for a geostationary satellite (d = 36 000 km), and a radio-relay system (d=50 km)

6.3 Phenomena associated to the Refractive Indexes

The refractive indexes of the media (troposphere, ionosphere, plasmasphere, etc.) where an electromagnetic wave successively travels vary along the direction of propagation. Accordingly, an electromagnetic wave will propagate along a curvilinear direction: in this case the wave is said to be refracted. From this phenomenon originate a number of different other effects: a lengthening of the path, changes in the propagation velocity or the angle of arrival, frequency variations, scintillations, etc.

Before turning to the study of these various phenomena, an understanding of the refractive indexes of the crossed media (troposphere, ionosphere) is necessary.

6.3.1 Troposphere

The refractive index n in the troposphere is defined from the meteorological parameters (pressure, temperature, humidity). It assumes a value close to unity and is generally characterised by his refractivity N connected to n by the following equation (see Chap. 3, Sect. 2.1):

$$N = (n-1)10^6 = \frac{77,6}{T}\left(P + 4810\frac{e}{T}\right) \text{ (N-unit)} \qquad (6.2)$$

where n is the refractive index, T is the temperature in K, P is the pressure (in hectopascals or in mb) and e is the water vapour partial pressure in hectopascals.

For further information on the subjects of modified refractive indexes, the standard atmosphere, space and temporal variability and the influence of atmospheric conditions, the reader is referred to Chap. 5 devoted to terrestrial fixed links.

6.3.2 Ionosphere

The refractive index in the ionosphere may assume different forms depending on whether the influence of the geomagnetic field and the influence of the collisions (absorption) between the electrons and atoms composing the propagation medium are taken into account. Different cases are therefore to be successively considered:

Non-absorbing medium not subjected to the influence of the terrestrial magnetic field

The equation for the refractive index in this case is:

$$n = \left(1 - \frac{Ne^2}{\varepsilon_0 m\omega^2}\right)^{1/2} = \left(1 - \frac{\omega_0^{\ 2}}{\omega^2}\right)^{1/2} = \left(1 - \frac{f_p^{\ 2}}{f^2}\right)^{1/2} \tag{6.3}$$

where:

- E is the electron charge,
- ε_0 is the permittivity of the medium,
- m is the mass of the electron
- N is the electronic density, i.e. the number of electrons per m^3,
- ω is the pulsation of the wave,
- $\omega_0^2 = \dfrac{Ne^2}{m}$ is the plasma pulsation,
- f_p is the plasma frequency in Hertz,
- f is the frequency, expressed as follows :

$$f_p = 9\sqrt{N} \tag{6.4}$$

Absorbing medium not subjected to the influence of the terrestrial magnetic field

The equation for the refractive index in this case is:

$$n = \left(1 - \frac{\omega_0^2}{\omega(\omega - j\nu)}\right)^{1/2} \tag{6.5}$$

where ν is the collision frequency.

Non-absorbing medium subjected to the influence of the terrestrial magnetic field

The equation for the refractive index becomes:

$$n = \sqrt{1 - \frac{\omega_0^2}{\omega^2 - \frac{\omega^2\omega_H \sin^2\theta}{2(\omega^2 - \omega_0^2)} \pm \sqrt{\omega^2\omega_0^2 \cos^2\theta + \frac{1}{2}\left(\frac{\omega^2\omega_H^2 \sin^2\theta}{\omega^2 - \omega_0^2}\right)^2}}} \tag{6.6}$$

where:

- $\omega_H = \dfrac{eB}{m}$ is the gyrofrequency,
- θ is the angle of propagation, i.e. the angle formed by the direction of propagation and the geomagnetic field.

Absorbing medium subjected to the influence of the terrestrial magnetic field

In such a medium, the equation for the refractive index is:

$$n = \sqrt{1 - \frac{\omega_0^2}{\omega(\omega - j\nu) - \frac{1}{2}\cdot\frac{\omega^2\omega_H \sin^2\theta}{\omega(\omega - j\nu) - \omega_0^2} \pm \sqrt{\omega^2\omega_0^2 \cos^2\theta + \frac{1}{2}\left(\frac{\omega^2\omega_H^2 \sin^2\theta}{(\omega - j\nu) - \omega_0^2}\right)}}} \tag{6.7}$$

Unlike in the troposphere, the refractive index here is lower than unity and is dependent upon the frequency. The refractive index thus defined is the phase index n_φ.

The following equation gives the group index, which is higher than unity:

$$n_g = \frac{1}{n_\varphi} = \frac{1}{\sqrt{1-\left(\frac{f_p}{f}\right)^2}}. \tag{6.8}$$

6.3.3 Refraction

The surfaces with equi-index *n(r)* are concentric around the Earth, since the refractive index *n(r)* is dependent on the distance from the Earth's centre. The paths followed by radio waves will therefore be defined by the following equation (see Fig. 6.2):

$$n(r).r.\cos\varphi = C^{te} \tag{6.9}$$

where r is the distance to the Earth's centre, φ is the refraction angle complementary to the incidence angle i, and $n(r)$ is the refractive index in the atmosphere.

The following equation defines the curvature at a point contained within the vertical plane:

$$\frac{1}{\rho} = \frac{-\cos\varphi}{n}\frac{dn}{dr} \tag{6.10}$$

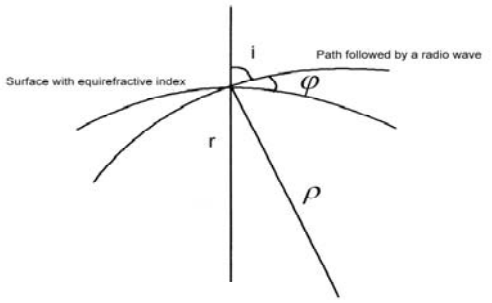

Fig. 6.2. Geometrical elements of the path followed by a radio wave

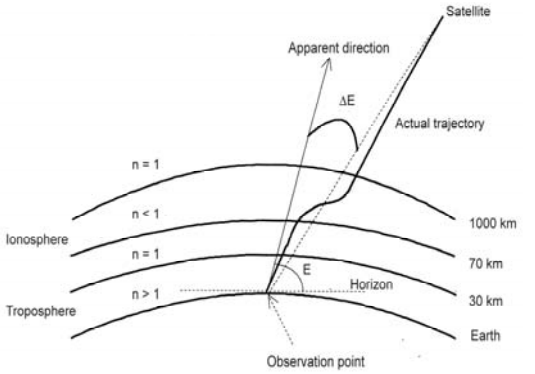

Fig. 6.3. Standard path between a satellite and the Earth

where:

- ρ is the radius of curvature of the ray path,
- n is the refractive index of the atmosphere,
- $\frac{dn}{dr}$ is the vertical gradient of the refractive index,
- φ is the angle to the horizontal direction of the ray path at the point under consideration.

The curvature of a ray is defined as being positive when its concavity is directed towards the Earth's surface.

In the troposphere, the vertical refractive index gradient is negative. Accordingly, the curvature of the paths will always be oriented along the same direction, and its concavity will be directed towards the Earth's centre.

In the ionosphere, the vertical refractive index gradient changes sign as the ray travels through the ionisation maximum: at this point, the curvature of the paths changes direction, as represented in Fig. 6.3.

6.3.4 Delay and Propagation Time Distortion

The propagation time from the satellite to the Earth is longer than the time calculated in free-space: indeed, the path actually followed by the wave is not rectilin-

ear and the wave propagates with a group velocity lower than the speed of light in vacuum. The resulting delay, known as the group delay or group propagation time, induces an error in the estimation of the distance from the source, in this case from the satellite. The following equation expresses the apparent lengthening of the path as a function of the geometrical path:

$$\Delta L = \int_0^S (n-1)ds \tag{6.11}$$

where s is the curvilinear coordinate on the path, n is the refractive index, and S is the distance separating the two extremities of the path (the terrestrial station and the satellite).

In the troposphere the path lengthening does not depend on frequency, but is affected by the meteorological conditions and decreases very rapidly with the angle of elevation. For elevation angles higher than ten degrees, the length difference can be expressed by the following equation (ITU-R P.834-2):

$$\Delta L = 0.00227 * P + \frac{1.79V}{T \sin\theta} \tag{6.12}$$

where:

- ΔL is the length difference in metres
- P is the atmospheric pressure in hPa or in mb,
- T is the temperature at ground level in K,
- θ is the elevation angle,
- V is the total water vapour content expressed in kg/m^2 or in millimetres of precipitable water.

Values for ΔL vary from 2.2 to 2.7 metres at sea level along the zenith direction. The reader will find statistics for V in Recommendation ITU-R P.836, along with a method for extracting the value of the total atmospheric water vapour content from radiometric measurements.

In the ionosphere the path lengthening depends on both the frequency and the total electronic content, as described by the following equation:

$$\Delta L \approx \frac{40}{f^2} \int_0^S N ds \tag{6.13}$$

where f is the frequency in MHz and N is the number of electrons (el/m^3).

In the case of a total electronic content (TEC) of 30*10^{16} el/m^2, the approximate lengthening at the 100 MHz frequency is of an order of 1200 metres.

Fig. 6.4 represents the variation of the path lengthening inside the ionosphere as a function of the frequency for different values of the total electronic content (10^{16}, 10^{17} and 10^{18} el/m^2). The dependency of the path lengthening on the frequency leads to a distortion of the propagation time and consequently to a deformation of the transmitted signals. The delay the wave undergoes is written in the form:

$$\Delta t = \frac{d\left(\frac{\Delta L}{c}\right)}{df} = \frac{80\Delta f}{cf^3}\int_0^S N ds \,. \tag{6.13}$$

The wave phase, being dependent on the total electronic content, varies in time, thereby inducing a Δf frequency shift:

$$\Delta f = \frac{40}{cf}\frac{d}{dt}\int_0^S N ds \tag{6.14}$$

The frequency of the wave received at ground level differs from the frequency emitted by the satellite. The apparent variations of frequency due to the ionosphere generally lie between 0.1 Hz (1.6 GHz) and a few Hertz in the case of low orbiting satellites emitting at 150 MHz.

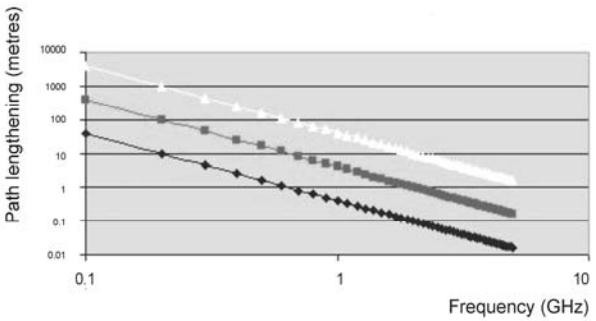

Fig. 6.4. Path lengthening in the ionosphere expressed as a function of the frequency for different values of the total electronic content: 10^{16}, 10^{17} and 10^{18} el/m^2

6.3.5 Direction of Arrival

The radio electric direction of the satellite differs from the geometrical direction by a ΔE value defined as follows:

$$\Delta E = \frac{(L + r\sin E)\, r\cos E}{h_i(2r + L) + (r\sin E)^2} \frac{\Delta L}{L} \tag{6.15}$$

where:

- L is the distance to the satellite,
- r is the Earth's radius,
- E is the apparent angle of elevation of the satellite, i.e. the angle as measured,
- h_i is the altitude of the electronic content average (300-450 kilometres).

6.3.6 Rotation of the Polarisation Plane

Due to the presence of the terrestrial magnetic field, the medium where the wave travels through is birefringent. Each component (ordinary and extraordinary) of the electric vector undergoes a different rotation. Consequently, a rotation of the polarisation plane of the linearly polarised wave can be observed as the wave reaches the boundaries of the ionosphere (Faraday effect):

$$\Delta\Omega = \frac{2{,}36 * 10^{-5}}{f^2} \int_0^S NB\cos\theta \sec\chi\, ds \tag{6.16}$$

where N is the total electronic content (TEC), B is the intensity of the terrestrial magnetic field, θ is the angle formed by the magnetic field with the direction of propagation, and χ is the solar zenith angle.

The values for $\Delta\Omega$ generally lie between 1 and 500 radians. Measurements conducted at several ground stations of the rotation of the polarisation plane of a wave emitted by a satellite have permitted the determination of the characteristics of itinerant ionospheric disturbances, such as their amplitude, their period, etc (Si-zun 1979).

6.3.7 Scintillations

As it travels inside the ionospheric medium, an electromagnetic wave undergoes rapid variations in its amplitude, phase and directions of arrival. These variations, called scintillations owing to the presence of irregularities inside the medium, are characterised by their depth, period and speed variation.

Different indices (S2, IF, etc.) have been defined for the study of scintillations:

$$S_2 = \frac{\overline{X}^2 - \left(\overline{X}\right)^2}{\left(\overline{X}\right)^2} \tag{6.17}$$

6.4 Attenuation by Atmospheric Gases

The transmission attenuation caused by atmospheric gases results from the molecular resonance of oxygen and water vapour.

An oxygen molecule has a single permanent magnetic moment. At certain frequencies, its coupling with the magnetic field of an incident electromagnetic wave causes resonance absorption. In particular, at frequencies around 60 GHz a coupling occurs between the intrinsic moment of the electron, its spin, and the rotational energy of the molecule, generating a series of absorption lines quite close to each other in the spectrum. These absorption lines come to merge, thus forming a single and broad absorption band. Fig. 6.5 represents the specific attenuation due to oxygen at different altitudes in the 50-70 GHz frequency range: the lower the pressure, the higher the resolution of the bands. Fig. 6.6 represents the specific attenuation coefficient due to atmospheric gases.

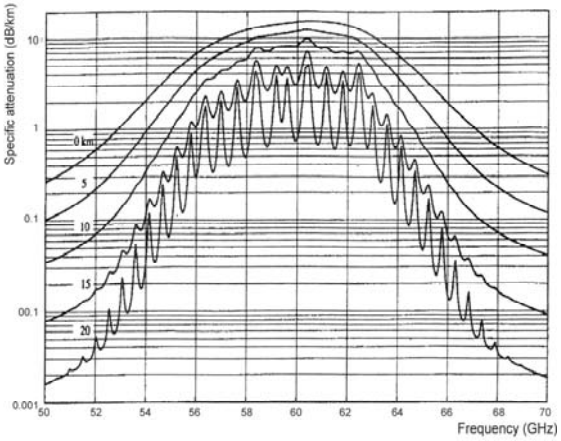

Fig. 6.5. Specific attenuation in the 50-70 GHz range at various altitudes (0, 5, 10, 15 and 20 km) (ITU-R P.676)

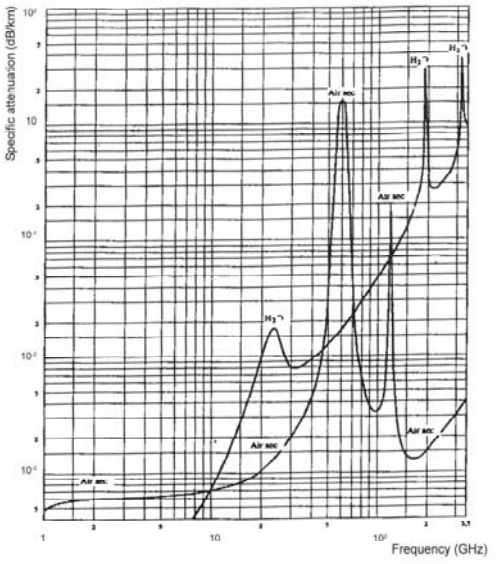

Fig. 6.6. Specific attenuation due to atmospheric gases (ITU-R P.676)

A water vapour molecule behaves like an electric dipole. The interaction of such a molecule with an incident wave disorientates the molecule by generating an additional internal potential energy. The attenuation maximum reached around the 22 GHz frequency is due to the resonance of the water molecule which starts to rotate while absorbing a high proportion of the incident electromagnetic energy.

The most accurate method for evaluating the attenuation due to atmospheric gases is by taking into account the contribution of all the absorption lines of oxygen and water vapour and the continuous spectrum of the absorption due to water and ice. Several models can be found in the literature (Liebe 1993; ITU-R 1999 Rec. ITU-R P.476-4; Salonen 1990; Gibbins 1986; Konefal et al. 1999).

The reference model, developed by Liebe et al., is known as the MPM93 model (Liebe 1993). This model allows determining the refractive index related to atmospheric oxygen and water vapour as well as the attenuation related to each of these components for frequencies up to 1000 GHz (Liebe 1981, 1985, 1989, 1993). The input parameters of this model are the pressure, the temperature, the relative humidity observed over a vertical profile of the Earth's atmosphere and the frequency (COST255 1999; ITU-R P.676-4).

As a numerical application of this model, the specific attenuation due to atmospheric gases in the case of an average atmosphere (7.5 g/m^3) was found to be equal to approximately 0.2 dB/km and 15 dB/km at 20 and 60 GHz respectively.

6.5 Hydrometeor Attenuation

The transmission attenuation due to hydrometeors like clouds, snow, fog or rain is caused by two factors: the energy absorption by Joule effect by hydrometeors and the wave diffusion induced by the particles.

6.5.1 Attenuation due to Clouds and Fog

Attenuation due to clouds and fog is determined on the basis of the total water content per volume unit. At frequencies around 100 GHz and at higher frequencies, fog attenuation may reach significant levels. The liquid water concentration is typically equal to approximately 0.05 g/m^3 inside a moderate fog (visibility of the order of 300 metres) and of 0.5 g/m^3 inside a thick fog (visibility of the order of 50 metres).

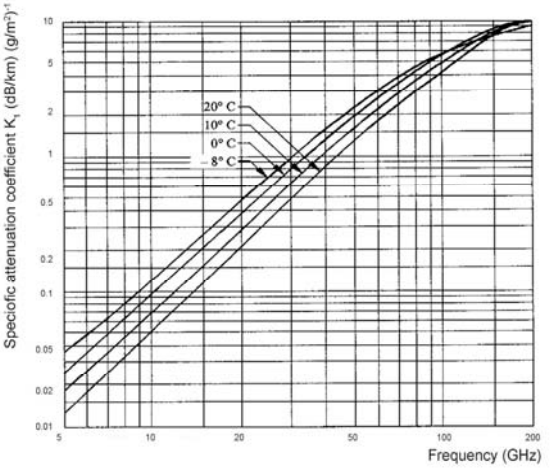

Fig. 6.7. Variation of the specific attenuation inside the cloud as a function of frequency (see Rec. ITU-R P.840)

In the case of clouds and fogs consisting entirely of very small droplets with diameter inferior to 0.01 centimetres on an average, the Rayleigh approximation is valid at frequencies lower than 200 GHz. Attenuation can therefore be expressed as a function of the total water content per volume unit (g/m^3).

The following equation yields the specific attenuation in clouds or fogs with such characteristics:

$$\gamma_c = K_l M \text{ (dB/km)} \tag{6.18}$$

where γc is the specific attenuation inside the cloud in dB/km, K_l is the specific attenuation in dB/km per g/m^3 and M is the concentration of liquid water in clouds or in fog in g/m^3.

Fig. 6.7 presents values for K_l at frequencies ranging from 5 to 200 GHz and temperatures varying between −8 °C and 20° C. For attenuation due to clouds, it is appropriate to use the curve corresponding to a 0° C temperature.

In the case of a moderate fog (0.05 g/m^3), the orders of magnitude for attenuation are 0.002 and 0.1 dB/km at the 20 and 60 GHz frequency ranges respectively, while for a thick fog (0.5 g/m^3) they reach 0.02 and 1 dB/km respectively.

In order to determine the attenuation due to clouds for a given probability value, it is necessary to know the statistics of the total content of liquid water L in kg/m^2 contained in a column or, equivalently, the total content of precipitable water in millimetres for a given site. The equation for attenuation can thus be written in the form:

$$A = \frac{L\ K_l}{\sin\theta} \text{ (in dB)} \quad \text{with } 90° \geq \theta \geq 5° \tag{6.19}$$

where θ is the angle of elevation, and the values for K_l are as reported in Fig. 6.7.

Statistics for the total content of a liquid water column can be obtained either from radiometric measurements or by launching radio-probes. If there are no local measurements available, it is advised, in order to calculate the attenuation due to clouds, to use the values of the total content of liquid water in a cloud column (normalised at 0° C) which can be collected from ITU-R data (ITU-R Rec. P.676). These data give the normalised content of liquid water in a cloud column (kg/m^2) exceeded during 20, 10, 5 and 1 percent of time over a year.

Let us describe a numerical application here: for a normalised total content of liquid water in a cloud column equal to 0.6 kg/m^2, a value exceeded during 1 percent of time over a year (average value in France), the zenith attenuation is equal to 0.25 and 1.2 dB at 20 and 60 GHz respectively. At an elevation angle of 45 degrees, the zenith attenuation is equal to 0.3 and 1.7 dB respectively, while at an elevation angle of 5 degrees it reaches 3 and 13 dB respectively.

6.5.2 Rain Attenuation

The determination of the attenuation due to rain relies more particularly on precipitation intensities (rainfall rates). Fig. 6.8 represents an example of the variation rate of the path loss in dB/km expressed as a function of the rainfall rate in mm/h obtained over an 800 metre horizontal link in Fontaine in France on May 31 1998, at the 30, 50, 60 and 94 GHz frequencies (Veyrunes 2000).

The specific attenuation γ_R (dB/km) is deduced from the rain rate R (mm/h) using the following power law equation:

$$\gamma_R = kR^{\alpha} \tag{6.20}$$

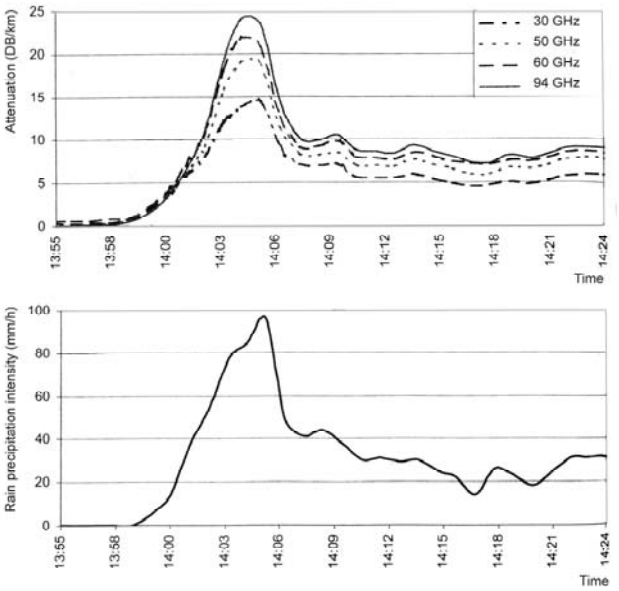

Fig. 6.8. Event of May 31, 1998: temporal rain attenuation (upper graph), temporal rainfall rate (lower graph)

The k and α coefficients depend on both the frequency and the polarisation (ITU-R P.837). Values for k and α can be obtained at different frequencies using a logarithmic scale for the frequency, a logarithmic scale for k and a linear scale for α.

For a 20 mm/h rain rate, a value exceeded during 0.1 percent of time in Belfort, rain attenuations is of the order of 2 and 8 dB/km at the 20 and 60 GHz frequencies respectively,. For a 40 mm/h intensity, a value exceeded during 0.01 percent of time, attenuation values are of the order of 3.2 and 13 dB/km respectively.

The Recommendation ITU-R, P.837 provides a model for the determination of the rainfall rate *Rp*, exceeded for any given percentage *p* of an average year, and for any given site. The same recommendation also gives examples of world charts for rain intensity (mm/h) exceeded during 0.01 percent of an average year. The data files were established on the basis of data collected for fifteen years by the *European Center of Medium-range Weather forecast* (ECMWF).

For long-term statistics concerning the calculation of rain attenuation over an oblique path for any given site, the reader is referred to Recommendation ITU-R P.618 §2.2.1.1. The input parameters are the point rainfall rate on the site over 0.01 percent of an average year (mm/h), the height above the average sea level of the ground station, the elevation angle, the latitude of the station, the frequency and the effective Earth radius. The method thus described is generally employed for the calculation of the scaling attenuation with parameters like the elevation angle, the polarisation and the frequency.

Concerning the problem of the long-term scaling in frequency and polarisation of the statistics for rain attenuation, the reader is referred to Rec. ITU-R P.618 §2.2.1.2.

A number of different models can be found in the literature. The reader will find in the COST255 final report, in addition to the ITU-R P.618 model, the most powerful models for rain rate forecasts, among which the Brazil model, the Bryant model, the Crane global model, the Crane two-component model, the DAH (Dissanayake-Alnutt-Haidara) model, the Excell model, the Flavin model, the Garcia model, the Karasawa model, the Leitao-Watson showery model, the Matricciani model, the SAM model, the Sviatogor model, the Assis-Einluft model or the Misme-Waldteufel model may be mentioned. Some of these models are detailed in Appendix I on rain attenuation.

Under the assumption that the rain to be homogeneous along the whole link, the attenuation corresponding to a given time percentage is obtained by multiplying the specific attenuation associated to the corresponding rain intensity for the same time percentage by the length of the link.

However, precipitation is generally intense only over relatively limited areas, at least in temperate climates. For this reason, rain cannot be assumed to be homogeneous. Rain attenuation could be calculated by integration from the distribution of the specific attenuation along the path using the equation:

$$A_{dB} = \int_{Path} \gamma(x) dx \tag{6.21}$$

Unfortunately neither the variation of rain intensity nor the specific attenuation along the path can actually be determined. Different practical methods have been proposed in order to account for the heterogeneity of rain. The most physical method consists in modelling intense rain areas, or rain cells. The implementation of this method requires a statistical representation of the dimensions of the cells as a function of rain intensity and even possibly to define a rain profile inside each cell, from its centre to its periphery. This physical model leads to relatively complicated calculations and would require a statistical knowledge of the structure of the rain which is far from being presently available.

The method universally employed at present is more empirical in character than the preceding, and is based on the equivalent path length notion. Assuming that the specific attenuation has already been determined, the attenuation along a path with length L is written in the form:

$$A_{dB} = \gamma kL = \gamma L_e \tag{6.22}$$

where L_e is defined as the equivalent length.

The equivalent length is always shorter than the geometrical length. This arises from the fact that attenuation forecasts are established over very small time percentages corresponding, due to the use of an equiprobability method, to high rain intensities, and the extension of such intensities is always inferior to the length of the link. The corrective factor k (or reduction coefficient required for passing from the effective distance to the hypothetical distance along which an uniform rain would fall) depends on the length of the link (with a value tending towards to unit for very short links where rain is almost homogeneous), and on the structure of the rain, i.e. on its intensity, as the latter is the only parameter allowing to characterise it. The following equation must therefore be satisfied:

$$\mathrm{k = k\ (L, R).} \tag{6.23}$$

Other relations have been suggested where the rain rate R is replaced by the considered time percentage P, leading therefore to the expression:

$$k = k(L, P). \tag{6.24}$$

As an illustration, we indicate hereafter two different formulas proposed for the determination of the corrective factor (Lavergnat 1997):

– the equation advanced by Lin on the basis of American data is of the first type and is written in the form:

$$k(L,R) = \frac{1}{1 + L\dfrac{(R-6.2)}{2636}} \tag{6.25}$$

– the equation advanced by Boithias (Boithias 1987) on the basis of European data is written in terms of time percentage rather than of rain intensity:

$$k(L,P) = \frac{1}{1 + 0.014\log(2/P)^{1.7}\,L^{0.9}} \tag{6.26}$$

6.6 Depolarisation Attenuation

Using orthogonal polarisations, two independent information channels with the same frequency can be transmitted along the same link. While in theory these two orthogonally polarised channels are completely isolated from each other, in reality a certain level of interference inevitably arises between them, due to the fact that the polarisation characteristics of the antennas are not perfect and to the depolarisation effects along the propagation path. Absorption and diffusion by hydrometeors are the main causes for the cross-polarisation that takes place at centimetric and millimetric wavelength ranges. These hydrometeors can be raindrops, ice, snow or hail. In the case of oblique satellite paths, all these different types of hydrometeors may be found along the path, either simultaneously or at different times and places. All these hydrometeors share the property of existing in a non-spherical form (for instance, the flattened shape of the large raindrops), thus creating different propagation characteristics (phase coefficient and specific attenuation) along the two principal axes. The two axes can generally be considered as orthogonal. The differential phase and attenuation effects due to hydrometeors thus modify the polarisation state of the radio waves propagated through the medium.

For instance, a linearly polarised wave whose polarisation plane is not aligned on any of the principal planes of the anisotropic medium will turn into an elliptically polarised wave. This means that a component perpendicular to the original wave, albeit out of phase with respect to it, has been produced. Therefore, a part of the energy will be transferred from the original polarisation (copolar channel) unto the orthogonal polarisation (cross-polar channel). The energy transfer which has thus taken place is measured by the discrimination ratio or decoupling polarisation factor (XPD) or by the cross-polarisation isolation factor (XPI). The definition and modelling of these different parameters are addressed at more depth in Appendix D devoted to the cross-polarisation caused by the atmosphere.

Table 6.1. Building penetration loss for different types of materials at the 17 and 60 GHz frequencies

Materials	17 GHz (V)	17 GHz (H)	60 GHz (V)	60 GHz (H)
Meshed glass	1.6 dB	0.03 dB	4.3 dB	0.6 dB
Glass	1.4 dB	0.9 dB	1.8 dB	2.2 dB
Plywood (3/4" thick)	5.6 dB	5.8 dB	12.7 dB	10.9 dB
Plasterboard (1/4" thick)	0.9 dB	0.8 dB	0.8 dB	2.6 dB
Two sheets of plasterboard	1.9 dB	1.8 dB	7.3 dB	6.4 dB
Thermolite block	54.7 dB	46.0 dB	56.8 dB	51.4 dB
Aluminium sheet (1/8" thick)	48.8 dB	43.2 dB	51.9 dB	42.3 dB

6.7 Building Penetration Loss

The building penetration loss is the power attenuation that an electromagnetic wave undergoes as it propagates from outside a building towards one or several places inside this building. This parameter is generally calculated by comparing the external field and the field present in different parts of the building where the receiver is located.

The value of the building penetration loss is influenced by a number of different physical parameters, whose effects intermingle most of the time. Among these different parameters the following are traditionally distinguished:

- the near environment : a distinction is drawn between districts with high towers more or less separated from each other and more traditional districts with buildings of average height,
- the reception depth in buildings: the amplitude of the field decreases as the mobile moves from the front of the building towards a room located inside it, while the influence of the inhomogeneities decreases as the penetration depth inside a building increases. Waves penetrate more easily through window panes than through brick walls. Accordingly, the paths followed by radio waves will be more or less attenuated, and might even be occulted.
- the incidence angle, which determines the reflection and transmission coefficients at a surface,
- the frequency,
- the nature of the materials : Table 6.1 presents numerical values of the attenuation of electromagnetic waves obtained for different types of materials at the 17 and 60 GHz frequencies and in horizontal *(H)* and vertical *(V)* polarisations respectively (Fiacco 1998). Further detail on this subject can be found in the final report by the RACE *Mobile Broadband System* project (RACE-MBS R2067 1999).

6.8 Attenuation due to the Local Environment

Depending on the angle of elevation, the local environment, for example in the form of buildings in suburban and urban media or of trees along roads in rural media, may prevent the propagation of radio waves.

6.8.1 Effects of Buildings

On the subject of the shadowing effects of buildings along roads, the reader is referred to Recommendation ITU-R P.681 4.2 where a model for the statistical probability of building shadowing with respect to the elevation angle, the average heights of the buildings, the height of the mobile and the distance between the mobile and the street, is presented.

6.8.2 Effects of Vegetation

An empirical model for representing the shadowing effect induced by trees along roads has been made available for the 2-30 GHz frequency range by the ITU-R (ITU-R P.681 4.1). In this model, the influence of the trees is represented by the percentage of optical shadowing resulting from their presence for a 45 degree elevation angle along the direction of the source of the signal.

In the case where the environment is known with an adequate level of precision (for example, if geographical base contour data are available), ray models can be

employed for the determination of the coverage area of a transmitter at any frequency.

The attenuation due to vegetation appears to increase with the frequency. However, while the ITU-R provides a few attenuation models in the UHF band, data available at frequencies higher than 10 GHz are few and scarce. This lack of results has been repeatedly stressed in the last recent years (Grindrod 1997; Seville 1997). Further, the existing results present quite different values for this parameter, depending on the type of vegetation under consideration.

An ancient ITU-R model gave the following equation for the excess attenuation due to vegetation:

$$A = \alpha f_{MHz}^{\beta} d^{\gamma} \tag{6.27}$$

where f is the frequency, d is the distance travelled inside vegetation and α, β, and γ are three parameters of the model (CCIR 1986).

A comparison between this equation and experimental measurements with the coefficients indicated by the CCIR yields a 22 dB standard deviation error (Seville 1997). Adjusting the coefficients permits to bring down the error to 11 dB. Taking into account the region simultaneously illuminated by the emitting and receiving antennas, the standard deviation error can be further reduced down to 8 dB (Seville 1997). In the aforementioned study, the author points out the great diversity of results, which depend on the type of vegetation: for instance, whereas for a spruce the transmitted wave attenuation is on an average equal to 10 dB, it is equal to 22 dB for a ficus at 40 GHz.

An experimental and theoretical study based on the energy radiative transfer theory (Schwering et al. 1988) was conducted at the 9.6, 28.8 and 57.6 GHz frequency ranges. This study reveals that the vegetation attenuation expressed in dB as a function of the distance d inside the vegetation increases linearly and rapidly, with rates ranging from 1.3 to 2 dB/m when d is relatively small, i.e. smaller than 30 metres. As d increases, the attenuation due to vegetation passes through a transition phase beyond which it still linearly increases, albeit at the slower rate of 0.05 dB/m. The explanation advanced is that this phenomenon results from the combination of the rapidly attenuated path with the more slowly attenuated diffused paths. If the diffused paths are predominant, the depolarisation of the waves can reach a high degree.

In some propagation models, the vegetation in urban areas is regarded as a shadowing region which prevents the propagation of electromagnetic waves (Correia 1996). At the 60 GHz frequency, the authors indicate values ranging from 6 to 8 dB for the attenuation due to vegetation (Correia *et al.* 1994).

A few qualitative results have been presented in a study realised at frequencies near 28 GHz by the US-WEST. According to this study, the attenuation due to vegetation may reach the order of several tens of dB. The excess attenuation due to vegetation and shadowing effects in suburban areas compared to free-space attenuation was found to have an average value, of interest from a statistical point of

view, equal to 4 dB/km with a 10 dB standard deviation at the 28 GHz frequency (US-WEST 1995).

The presence of vegetation is also the cause of the fast fading of the received field, correlated with the speed of the wind. In narrow band, an adjustment of this fast fading can be performed using a Rice-type law (US-WEST 1995). The study conducted by US-WEST shows that in this case the Rice parameter is correlated to a reasonable extent with the additional attenuation due to vegetation.

Measurements of the attenuation of the signal have also been carried out at the 60 GHz frequency in forest areas along roadside trees whose branches extend over the road (Grindrod *et al.* 1997). The transmitter is therefore only partially in line-of-sight. Up to a distance equal to 20 metres, the attenuation due to the foliage hanging over the road is no higher than 5 dB. Beyond this distance, strong variations of signal can be observed, which are explained by the authors by the interferences arising between the direct path attenuated by the leaves and the diffused paths. When the transmitter is placed directly behind a group of conifers, the attenuation reaches values ranging from 30 to 50 dB, corresponding to distances inside vegetation ranging from 60 to 80 metres.

In addition, the crossing of vegetation causes a depolarisation of the waves in direct proportion to the additional attenuation that it induces. For an initial isolation value of 24 dB between the two horizontal and vertical polarisations in free-space propagation, experiments carried out by the US-WEST have shown that the isolation of the two polarisations decreases by 1 dB when the additional attenuation due to vegetation rises by 3 dB. It suggests that the depolarisation effect due to vegetation is much more important than the depolarisation due to rain.

For further detail on the evaluation of attenuation due to vegetation, the reader is referred to Appendix J on vegetation attenuation.

References

Boithias L (1987)) Radiowave Propagation, Mc Graw-Hill, New-York

COST 255 (1999) Radiowave propagation modelling for Satcom services at Ku-band and above. COST255 Final Wokshop, Bech, Luxembourg

Fiaco M, Parks H, Radi H, Saunders SR (1998) Indoor Propagation factors at 17 and 60 GHz. Final report by the Centre for Communication Systems Research on behalf of the Radiocommunications Agency

Foulonneau B, Glangetas E, Bic JC (2000) Characteristics and reflection scattering profile of building materials in the 60 GHz band for indoor propagation prediction tools. AP2000, Davos

Gibbins CJ (1986) Improved algorithms for the determination of specific attenuation at sea level by dry air and water vapour in the range 1-350 GHz. Radio Science 21 6: 945-954

Grindrop EA, Hammoudeh A (1997) Performance characterisation of millimetre wave mobile radio systems in forests. 10th ICAP pp 2.391-2.246

ITU-R P.618 Propagation data and prediction methods required for the design of Earth-space telecommunication systems

ITU-R P.676 Attenuation by atmospheric gases
ITU-R P.833 Attenuation in vegetation
ITU-R P.834 Effects of tropospheric refraction on radiowave propagation
ITU-R P.837 Characteristics of precipitation for propagation modelling
ITU-R P.839 Rain height model for prediction methods
Lavergnat J, Sylvain M (1997) Propagation des ondes radioélectriques. Introduction. Masson, Paris
Liebe HJ (1983) Modeling attenuation and phase of radio waves in air at frequencies below 1000 GHz. Radio Science 16:183-1199
Liebe HJ (1985) An updated model for millimetre wave propagation in moist air. Radio Science 20 5: 1069-1089
Liebe HJ (1989) MPM - An atmospheric millimetre-wave propagation model. Int. Journal of infrared and millimetre waves, 10: 631-650
Liebe HJ, Hufford GA, Cotton MG (1993) Propagation modelling of moist air and suspended water/ice particles at frequencies below 1000 GHz. AGARD 52nd Specialists meeting of the EM wave propagation panel, Palma de Maiorca
RACE-MBS (1999) Final report on propagation aspects. R067/IST/2.2.5/DS/P/070.b1
Salonen E *et al.* (1990) Study of propagation phenomena for low availabilities. ESA/ESTEC Contract 8025/88/NL/PR, Final report
Schwering FK, Violette EJ, Espeland RH (1988) Millimetre wave propagation in vegetation: experiments and theory. IEEE Trans. On Geoscience and remote sensing vol 26 3: 355-367
Seville (1997) Vegetation attenuation : modelling and measurements at millimetric frequencies, 10th ICAP: 2.5-2.8
Sizun H (1979) Les perturbations ionosphériques itinérantes de moyenne échelle, étude et recherche de leur source. PhD Thesis, Université de Rennes
US WEST Advanced Technology Inc, HP Company; (1995) Final Report of the LMDS Phoenix Field Trial. Report T-09_02-004963-01.00